Journal of Physics: Conference Series **591** (2015) 012011 doi:10.1088/1742-6596/591/1/012011

Neoclassical modeling of the radial electric field and comparison with measurements in the TJ-II stellarator

C. Gutiérrez-Tapia[1], J. J. Martinell[2], D. López-Bruna[3], A. V. Melnikov[4]

[1] Instituto Nacional de Investigaciones Nucleares, México
[2] Instituto de Ciencias Nucleares (UNAM), México D.F., México
[3] Asociación EURATOM-CIEMAT, Madrid, Spain
[4] Research Centre Kurchatov Institute, Nuclear Fusion Institute, Moscow, Russia

E-mail: cesar.gutierrez@inin.gob.mx

Abstract. The results of the radial electric field measurements by Heavy Ion Beam Probe (HIBP) in the TJ-II stellarator are compared with neoclassical transport computations. The role played by several plasma features is identified by studying a reduced analytical transport model, using both actual density and temperature profiles and representative model profiles for varying density. Additional electric field calculations are carried out numerically with the Astra code using three different expressions for the neoclassical transport coefficients in order to identify the common features characterizing E_r, particularly the sign reversal. For regimes with a wide variation of collisionality, a general qualitative agreement between modeling and experimental data is shown. The obtention of roots for E_r depends critically upon the temperature and density profiles as they determine the plasma collisional regime. It is found that the root transition (i.e. E_r sign reversal) occurs for a specific range of a collisionality parameter, consistent for all models employed. It is found that when density and temperature profiles give real roots of the electric field the pressure is almost constant. Discharges with high radial gradient of E_r are found to correlate well with high confinement regimes.

1. Introduction

In non-axisymmetric magnetic configurations like those of stellarators, the NC contribution is crucial in the analysis of phenomena related to E_r. Indeed, there have been joint efforts to proceed to a benchmark of numerically obtained NC electric fields and fluxes with experimental data in conditions suitable for a NC treatment [1]. In the particular case of the TJ-II device, an acceptable agreement between experiments and Montecarlo calculations has been obtained in low density regimes [2, 3]. Additionally, some works were dedicated to compare a particular formulation of the NC fluxes to describe the electric fields with experiment in restricted plasma conditions [4, 5].

Since the conditions and basic statements of NC theory are well grounded and provide a first approximation to transport, it is desirable to have practical implementations that evaluate this important contribution on transport and especially on the ambipolar radial electric field. The present work is also benchmark-minded, but from a more immediate and practical perspective: it is based on easy-to-implement formulations of the NC particle fluxes. The objective is to

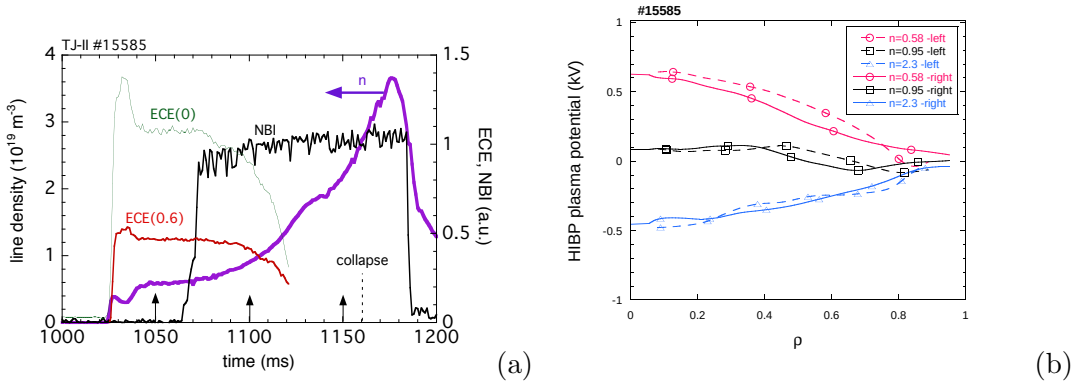

Figure 1. (a) Time signals of Electron Cyclotron Emission (ECE) from the magnetic axis and from $\rho = 0.6$, line density $\bar{n}$ through the magnetic axis and NBI heating during an NBI discharge (TJ-II #15585) with continuous density rise. The ECE signals drop when the ECE cut-off is reached at $\bar{n} \approx 1.2 \times 10^{19}$ m^{-3} but the plasma remains hot until the radiative collapse at $t \approx 1160$ ms. (b) Plasma potential profiles corresponding to the times indicated with the arrows in (a).

provide a practical tool for the evaluation of the radial electric field under the assumptions that (i) the main non-ambipolar radial fluxes are of neoclassical origin and (ii) the functional dependencies of such fluxes for electrons and ions are enough to obtain E_r even if the fluxes themselves are not accurately described. If the results obtained from the NC formulations are found to be consistent with the experimental results, this model should be suited as a tool for the interpretation of experimental data, and also for predictive estimates. For this to be trustworthy, not one but different formulations of the NC problem should yield consistent and robust results with respect to the experimentally found trends of the radial electric field. We believe that this is especially significant when the exercise is done with plasmas operated in a complex magnetic geometry like that of a Heliac device, as the TJ-II is.

2. Experimental data

The TJ-II Heliac-type stellarator has a helical magnetic axis that winds around a circumference of radius $R_0 = 1.5$ m. The plasma has a bean-shaped cross section with average minor radius of $a \approx 0.2$ m and magnetic field at the axis $B_0 \approx 1.0$ T. The plasmas are always initiated with Electron Cyclotron resonance Heating (ECH); absorbed heating powers are normally $P_{\rm ECH} = (200 - 400)$ kW and in the absence of other heat sources the line averaged densities are $\overline{n} = (0.3 - 1.0) \times 10^{19}$ m^{-3} with central electron temperatures $T_e(0) \sim 1$ keV and ion temperatures of $T_i(0) \sim 0.1$ keV due to Coulomb heat exchange. Additional heating and fueling can be obtained with the help of one or two neutral beam injectors (NBI) delivering port-through powers $P_{\rm NBI} = (300 - 600)$ kW each. Above line densities of around 1.2×10^{19} m^{-3} the ECH is no longer effective and the plasmas are sustained with NBI heating alone up to densities $\overline{n} = (2.0 - 6.0) \times 10^{19}$ m^{-3} with lower temperatures: $T_e(0) \lesssim 0.3$ keV and $T_i(0) \sim 0.5 T_e(0)$.

The electron density and temperature profiles are measured using the Thomson Scattering diagnostic from the magnetic axis up to $\rho \approx 0.7$, where ρ is the normalized flux surface label proportional to the enclosed plasma volume. In order to obtain the density profiles, interferometry and reflectometry data are used to extend the profiles to the edge ensuring that their line integral matches the experimental value. The ion temperature is normally measured with the CX neutrals analyzer. $T_i(\rho)$ is quite homogeneous in the low density ECH plasmas and

thus very different from T_e profiles due to the low collisional coupling in these cases. In what follows, we use T_i based on the central values provided by the diagnostic. The plasma potential in the bulk plasma is measured using the HIBP system described in [6].

Fig. 1(b) shows the plasma potential profiles $\phi(\rho)$ that correspond to the times indicated by vertical arrows in figure 1(a). Two profiles are shown at each density value because the diagnostic takes measurements at both sides of the magnetic axis (labelled 'left' and 'right'). This will be used as an indication of the uncertainty in the evaluation of the plasma potential. During the ECH phase $\phi(0)$ is positive with values in the 400–1000 V range that depend on $\bar{n}$. At high enough densities still in the ECH phase, the plasma potential becomes negative near the plasma edge and causes also the appearance of negative electric fields around the region of maximum density gradient [7]. In discharge #15585 this happens during the mixed ECH+NBI phase, when $\bar{n}$ increases, T_e decreases and T_i also experiences a small ($\sim 20\%$) rise correlated with the increased density. At still larger densities, like in the pure-NBI phase, $\phi(0)$ becomes negative as in the rest of the plasma. When $\bar{n} \approx 2 \times 10^{19}$ m^{-3}, the plasma potential is negative everywhere reaching values between -300 and -600 V near the magnetic axis. It should be noted that the change of sign of the plasma potential occurs in a rather continuous way starting near the edge where $T_e \sim 50$ eV and moving towards the center as n increases.

According to figure 1, three different types of plasma have been considered that represent different collisionality regimes and can be characterized by the corresponding average electron density:

LDHT (low density with high electron temperature): Low density ($\sim 0.6 \times 10^{19}$ m^{-3}), high electron temperature ($T_e(0) \sim 1$ keV) and low ion temperature ($T_0 \sim 0.1$ keV) as normally found in ECH plasmas. This regime is characterized by long mean free paths (LMFP) of the particles over most of the plasma, $\nu^* \ll 1$, giving rise to radial fluxes dominated by the contribution of bouncing trapped particles in the large magnetic ripple. Here, $\nu^* = \nu/\omega_t$ is the collision frequency normalized to a model transit frequency $\omega_t = v_{th}/(R_0 q) = \iota v_{th}/(2\pi R_0)$, involving the rotational transform in radians ι and the thermal speed v_{th}. In this regime the electrons, being much faster than the ions and having large magnetic moment due to the heating system (ECH), dominate the radial fluxes causing E_r to be positive and $\phi \sim T_e/e$ in the plasma core. The plasma potential is then positive over the entire plasma column.

IDT (intermediate density and electron temperature): Intermediate densities ($\sim 10^{19}$ m^{-3}) and electron temperatures ($T_e(0) \sim 0.5$ keV), typically found in mixed ECH +NBI plasmas, or in high density ECH plasmas. The electron temperatures are lower than in the typical ECH plasma, while T_i remains on the order of 0.1 keV. This regime is known from the first TJ-II experimental campaigns for inverting the sign of the plasma potential (inferred from floating potential measured with electric probes [8]), as well as the electric field (according to spectroscopic measurements of plasma rotation [9]) somewhere inside the plasma. In particular, E_r starts becoming more negative near the plasma edge [7]. With increasing average densities, the negative values of E_r cover also smaller radii.

HDLT (high density and low electron temperature): High density ($\gtrsim 2 \times 10^{19}$ m^{-3}) and low temperatures ($T_e(0) \lesssim 0.3$ keV, $T_i(0) \lesssim 0.14$ keV), corresponding to NBI plasmas. When the density is further increased from the IDT regime, the plasmas have closer electron and ion temperatures and high density giving rise to shorter mean free paths for electrons and ions, satisfying $\nu^* \lesssim 1$, ions being closer to one. The contribution from helically trapped particles is now much smaller and the radial transport in these conditions is probably dominated by passing and toroidally trapped particles over a large portion of the plasma column, which corresponds to the "plateau" regime. The larger tendency of ions to escape the plasma causes $E_r < 0$ in the entire plasma column.

Figure 2 shows density (a) and electron temperature (b) profiles taken from the same

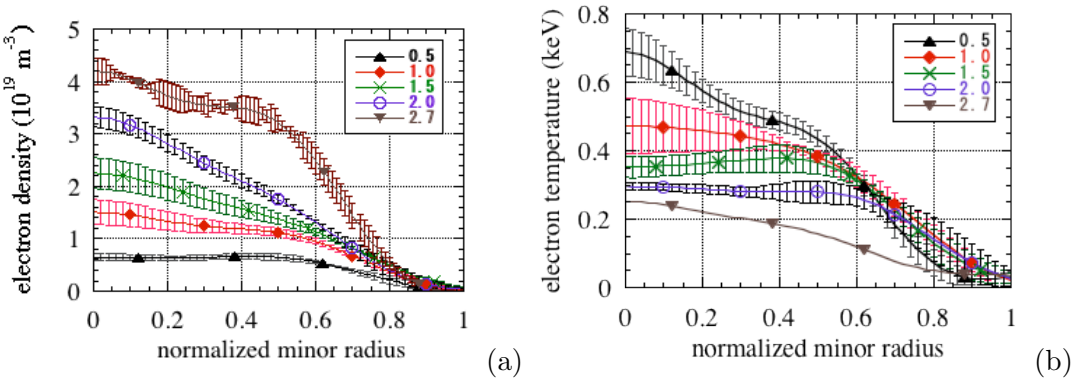

Figure 2. Averages of Thomson Scattering profiles at different line densities $\bar{n}$ (10^{19} m^{-3}) taken from N sample discharges according to the $\bar{n}(N)$ sequence 0.5(6), 1.0(6), 1.5(3), 2.0(5), 2.7(1). Large error bars in $T_e(\rho > 0.8)$ at $\bar{n} = 2.7$ have not been drawn for clarity.

experimental day of discharge #15585 (Fig. 1) at fixed line densities within a 10% range, with values (0.5, 1, 1.5, 2 and 2.5 in 10^{19} m^{-3} units). The profiles shown correspond to averages of Thomson Scattering profiles based on N discharges, with N = (6, 6, 3, 5 and 1) respectively — only one discharge was available for the highest density. Each individual profile is obtained after fitting a short expansion (typically 4th or 5th order) of Bessel functions in order to obtain $T_e(\rho)$ and $n_e(\rho)$ with reasonably smooth radial derivatives. Note that Thomson Scattering profiles are obtained from 256 points in the TJ-II diagnostic that show a fine structure [10], while in the present study we are only interested in the main macroscopic variations. The error bars in Fig. 2 are the standard deviation of the corresponding N profiles, except for the highest density case, where the errors obtained from Bayesian analysis [11] are shown for the only available discharge. Incidentally, this shows that these two errors are similar. The profiles and their radial derivatives are then mapped to a same calculation grid $[\rho_j]$. The ion density n_i is slaved to n_e through a prescribed effective charge $Z_{\rm eff} = 1.2$.

Table 1. Constant values appearing in expressions (1) for different regimes of electron density and temperature ((a) LDTH regime, (b) IDT regime, and (c) HDLT regime) obtained from the fitting to an hyperbolic curve $T_{e0} = 1/(0.9226 + 0.7623 n_{e0})$. Densities are expressed in 10^{19}m^{-3}, and electron and ion temperatures in KeV.

	n_a	n_0	a	b	T_{ae}	T_{0e}	a_e	b_e	T_{ai}	T_{0i}	a_i	b_i
LDHT	0.11	≤ 1	6.21	4.07	0.01	$(0.65, 0.7)$	1.9	1.66	0.01	0.077	40	10
IDT	0.08	$(1, 2)$	2.27	1.23	0.02	$(0.45, 0.5)$	2.91	1.64	0.01	0.09	35	10
IDT	0.09	$(2, 3)$	1.34	1.02	0.04	$(0.35, 0.4)$	6.64	5.43	0.01	0.09	35	10
IDT	0.11	$(3, 4)$	1.53	1.58	0.02	$(0.3, 0.35)$	5.23	2.12	0.01	0.09	35	10
HDLT	0.09	$(4, 5)$	4.78	5.11	0.02	$(0.25, 0.3)$	2.15	2.40	0.01	0.11	30	10

Finally, and since an algebraic model will be used later, we have prepared a set of analytic profiles that reproduce the main features of the experimental ones shown in Fig. (2), having the

form

$$n(\rho) = n_a + n_0(1-\rho^a)^b; T_e(\rho) = T_{ae} + T_{0e}(1-\rho^{a_e})^{b_e}; T_i(\rho) = T_{ai} + T_{0i}(1-\rho^{a_i})^{b_i}, \quad (1)$$

where n_a, T_{ae}, and T_{ai} are the electron density, electron temperature and ion temperature at the boundary, while n_0, T_{0e} and T_{0i} give the corresponding values at the center. Since the corresponding central values of the experimental data shown in Fig. 2 can be well fitted by an inverse relation, $T_{e0} = 1/(0.9226 + 0.7623 n_{e0})$, as shown in Fig. 3(a), we have taken n_0, T_{0e} to fall on this curve. The parameters a and b in Eq. 1 selected for our calculations are given in Table 1. They produce the profiles shown in Figs. 3(b) and 4, where the model profiles are compared with the experimental ones.

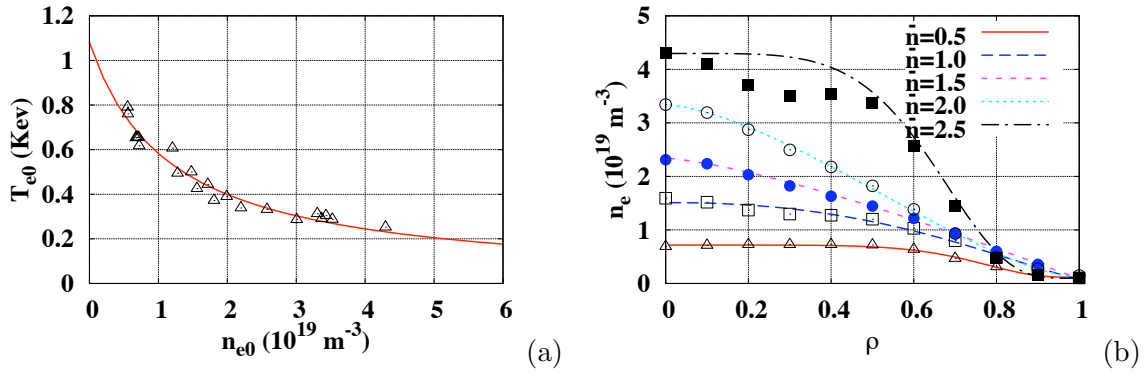

Figure 3. (a) Measured central electron temperature as function of central density showing hyperbolic- like dependence; (b) density profile: LDHT regime (solid line) and experimental (empty triangles), IDT regime (dotted lines) and experimental (empty squares, filled and empty circles), and HDLT regime (dash-dotted line) experimental (filled squares).

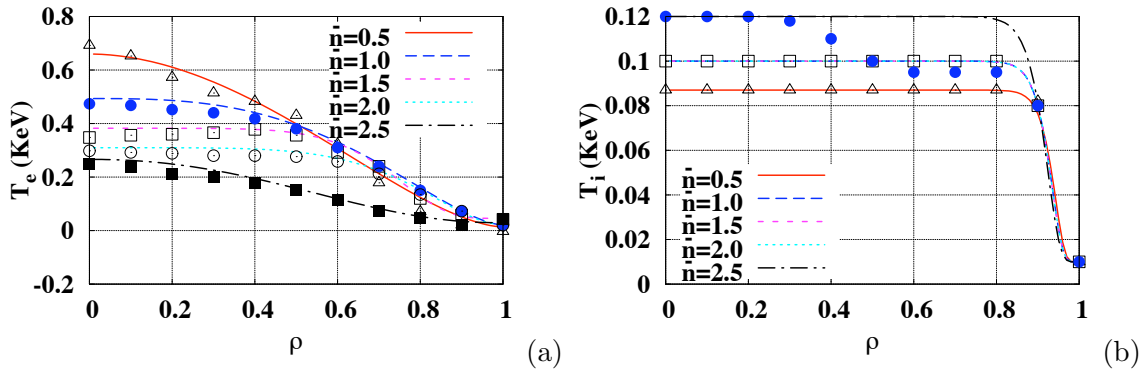

Figure 4. (a) Electron temperature: LDHT regime (solid line) and experimental (empty triangles), IDT regime (dotted lines) and experimental (empty squares, filled and empty circles), and HDLT regime (dash-dotted line) experimental (filled squares); (b) Ion temperature: LDHT regime (solid line) and experimental (empty triangles), IDT regime (dotted line) and experimental (empty squares), and HDLT regime (dash-dotted line) experimental (filled circles).

3. Neoclassical calculations of the radial electric field

The radial electric field in a stellarator can be computed from the neoclassical transport theory, starting from the diffusive fluxes for ions and electrons, Γ_j (with $j = e, i$). These fluxes have been calculated from kinetic theory or a two-fluid description to obtain closed forms in terms of the plasma parameters by several authors [12, 13, 14, 15]. From the dependence $\Gamma_j(E_r)$ it is possible to compute the radial electric field by applying the ambipolarity condition. Here we use three different formulations of the neoclassical fluxes to obtain E_r following certain procedures that numerically integrate the analytical formulas. For the algebraic model described below, the first procedure solves directly the ambipolarity equation

$$\Gamma_e(E_r) = Z_i \Gamma_i(E_r). \tag{2}$$

to determine E_r (additional conditions may be necessary if multiple roots exist for Eq. 2 which may produce a discontinuity of E_r as function of the radial coordinate). The other procedure, which is more convenient from the numerical point of view, follows the evolution of the electric field solving the equation

$$\frac{\partial E_r}{\partial t} \approx \frac{|e|}{\varepsilon_\perp} \left(\Gamma_e - Z_i \Gamma_i\right) \tag{3}$$

until the steady state is reached, which gives E_r. Here, $\varepsilon_\perp$ is the perpendicular dielectric constant and it is assumed that a term representing electric field diffusion is small [16]. Additionally, E_r is obtained from a simplified formulation due to Kovrizhnykh [17] which allows to follow an algebraic procedure to compute the electric field. For this model, E_r comes from the solution of a cubic equation which follows from Eq. 2.

The models used in this work simplify the complicated magnetic geometry in stellarators to obtain tractable NC transport fluxes, with the consequence that the resulting formulas do not give a full account of them, but they can be used to calculate E_r. No attempt is made to match the observed radial transport since it usually has an important anomalous component, particularly in regions far away from the plasma core. Since the non-ambipolar fluxes are mainly neoclassical, we expect that the E_r obtained from NC transport explain the measured values reasonably well. The ability to reproduce the electric field should depend on the way the NC fluxes react to this field, which is different in the various models considered.

3.1. Semi-analytical models for the neoclassical particle fluxes

Beidler's model. The first model provides mono-energetic transport coefficients for an idealized stellarator field with a single helical mode (see Eq. 4 below) obtained by Beidler [18, 19] from fits to DKES calculations. This model smoothly connects the three collisionality regimes that arise from the analytical theory of transport in a stellarator (ν, $\sqrt{\nu}$ and $1/\nu$), together with the axisymmetric transport, which becomes dominant at large collision frequencies. The monoenergetic transport coefficients have to be integrated over the thermal velocity distribution.

Kovrizhnykh's model. A second model reported by Kovrizhnykh [20], expresses particle fluxes as due to the contributions of an axisymmetric part Γ_j^S and an asymmetric one Γ_j^A (i.e. non-axisymmetric) for both the electrons ($j = e$) and ions ($j = i$), $\Gamma_j = \Gamma_j^S + \Gamma_j^{AS}$. The two parts have expressions that depend on the collisionality regime and Kovryzhnikh has derived interpolation formulas that are approximately valid for all the regimes. Formulas for the radial fluxes, were given in terms of the thermodynamic forces and the magnetic helical ripple ϵ_h entering the assumed representation for the standard stellarator magnetic field with a single helical harmonic,

$$B_T = B_0(R_0/R)[1 - \epsilon_h(r)\cos(l\theta - M\varphi)]; \quad \epsilon_h(r) = \epsilon_0 I_l(Mr/R_0). \tag{4}$$

In these expressions, ϵ_0 is a constant defining the amplitude of the stellarator field, related to $\iota(0)$, and $I_l(x)$ is the modified Bessel function of the first kind

The particle fluxes are based on a derivation that correctly describes the ambipolar field and the parallel (to $\mathbf{B}$) plasma velocity [14], and are given by expressions interpolated over the collisionality regimes for the symmetric and asymmetric components listed in [20].

Shaing's model. There is a third model presented in [12, 13]. In these reports authors argued that several values of the radial electric field can be possible that satisfy the ambipolar equation, but some of them are unstable. Thus, to find a stable solution for E_r from the thermodynamic point of view, this field must be at the minimum of the generalized heat production rate. Here, helical and toroidal ripples appear explicitly in the magnetic field taken of the form $B = B_0\left[1 - \epsilon_t \cos\theta - \epsilon_h \cos(l\theta - m\phi)\right]$, giving the asymmetric transport fluxes [13]. The symmetric part in this case is intrinsically ambipolar and is given by the usual expressions for axisymmetric devices [15]. The electric field is obtained solving Eq. 2.

The magnetic geometry in the models is taken from typical equilibrium computations and does not intend to capture the detailed geometry of the TJ-II device, but the main tendencies of collisional transport should be preserved. Profiles for the rotational transform ι and ripple amplitudes $\epsilon_{t,h}$ follow from those computations. For analytical uses the ripples are taken as

$$\epsilon_t = \alpha_t \rho^{\beta_t}; \quad \epsilon_h = \alpha_h \rho^{\beta_h}, \tag{5}$$

where the parameters $\alpha' s, \beta' s$ can be chosen to fit experimental data to account partially for geometrical effects. We will use $\alpha_t = 0.095, \beta_t = 0.55$ [21], but α_h and β_h will be used as free parameters to improve the fit of the E_r profiles.

In all these models the radial electric field enters only the non toroidally symmetric part since in a tokamak-like geometry steady state particle fluxes are ambipolar. The models are strictly valid for steady state conditions since no time dependent terms due to polarization drifts are included.

3.2. Algebraic formulation

Here we present an analytical model based on a reduced representation of Kovrizhnykh formulas, which allows to find the roots of the ambipolar equation (2) in closed form for given plasma profiles. The process followed is to give the model profiles of Eq. 1 for $n(\rho), T_e(\rho)$ and $T_i(\rho)$, compute the fluxes Γ_e and Γ_i and obtain E_r from Eq. (2). This simplified analytical model [17] assumes a simple magnetic geometry with a single helical harmonic. For the helical ripple we have taken ϵ_h with the values given after Eq. 5. The NC fluxes used are more appropriate in a low collisionality regime where the most important contribution to the transport coefficients comes from particles locally trapped in the helical ripple wells.

It is assumed that axisymmetric and anomalous fluxes are ambipolar and then only the asymmetric contribution is relevant: $\Gamma_j = \Gamma_j^{AS}$. In a quasi-stationary state with external particle sources Γ^{ext}, the particle balance equation

$$\Gamma_j = \Gamma^{ext} \tag{6}$$

has to be solved together with the ambipolarity equation (2). But in our analytical approach, only equation (2) is considered which gives an algebraic equation of third degree in the dimensionless electric field V. This can be solved once the equilibrium profiles $n(\rho)$ and $T_j(\rho)$ are given. However, not all profiles are physically possible, since the requirement of a single real root for $V = q_i E_r / T_e$ for all radial positions limits the choice of values of the profile parameters. This profile constriction can be understood, according to [17], in terms of the required particle sources obtained from Eq. (6) for the set of profiles $V(\rho), n(\rho)$ and $T_j(\rho)$. When V is not real

and continuous the sources are not physically acceptable and then the profiles are not possible. The equation for the electric field V in steady state coming from Eq.(2) can be written as,

$$F(\rho, V) = V^3 + b(\rho)V^2 + c(\rho)V + d(\rho) = 0. \tag{7}$$

where the coefficients $b(\rho)$, $c(\rho)$, and $d(\rho)$ are given in [17]

Depending on the values of the coefficients $b(\rho)$, $c(\rho)$, and $d(\rho)$, equation (7) can have up to three roots, $V_1(\rho), V_2(\rho), V_3(\rho)$. In general, two roots are stable and one is unstable, but they have to be real in order to be acceptable. If the profiles are set arbitrarily, the solutions in certain regimes can present a jump in the E_r profile that corresponds to the transition from one root to another. As pointed out by Kovrizhnykh [17], this requires particle sources of the Dirac delta function type at the discontinuities, which is unphysical. Therefore, these solutions should be discarded arguing that the corresponding $T_j(\rho)$ and $n(\rho)$ profiles cannot be obtained. The profiles that have been verified to yield one real root solutions for E_r all over the plasma have central values of density and electron temperature that fall on the hyperbolic curve shown in Fig. 3(a). This assures that the ambipolarity condition is satisfied at each magnetic surface. The density and temperature profiles corresponding to the values given in Table 1, for each of the regimes defined in § 2 satisfy this criterion and are shown in Figs. (3(b), 4(a), 4(b)).

4. Comparison with experimental data

4.1. Semi-analytical models.

Here we present the results for the three models described in Sec. 3.1. The NC particle fluxes are obtained using the formulas for each model, and the radial electric field is obtained with a numerical code coupled to the ASTRA transport shell [22] that starts with an initial E_r, normally $E_r(r) = 0$, and evolves the equation (3) in every radial position r_j until a steady state is reached. When the experimental profiles of Fig. 2 are used the profiles obtained for the radial electric field are shown in Fig. 5. They are computed for three representative densities using each of the models, and the experimental electric field profiles are also shown for comparable densities computed from HIBP data of the electric potential. The experimental E_r-profiles can be matched better using $\epsilon_h(\rho)$ as a "fitting function". However, the purpose of this work does not require finding a "best fit" but a reasonably good behavior.

Since the potential is the quantity actually measured by HIBP we focus on the physical scalings of $\phi(\rho)$. The dependency with density is represented in a plot of the central potential which is the most sensible to density. The results of the three models can be seen in Fig. 6 when the experimental density and temperature profiles given in Fig. 2 are used. It shows that the behavior of all of the models is quite similar. We recall that the parameter ε_h has been adjusted to improve the fits in each model, thus allowing the good agreement among them. The values for the analytical computations are also shown for comparison. The shadowed region in the graph indicates the range of experimental values from HIBP and shows that the semi-analytical models are able to reproduce the measurements to some extent. At intermediate densities the agreement is good and a small departure is seen for low densities due to effects not included in the NC model such as the presence of suprathermal electrons. The values of the density for the potential sign change are almost the same for all models. Shaings's model gives somewhat smaller $\phi(0)$ values. It is worth mentioning that the smaller values of $|E_r|$ (and $|\phi|$) found in the HDLT case with the semi-analytical models coincides with the results found numerically based on Montecarlo calculations, which also underestimate the magnitude of E_r [1]. However it is noteworthy that the saturation of $|E_r|$ seen at high density is well reporduced by all models although the asymptotic value is model dependent.

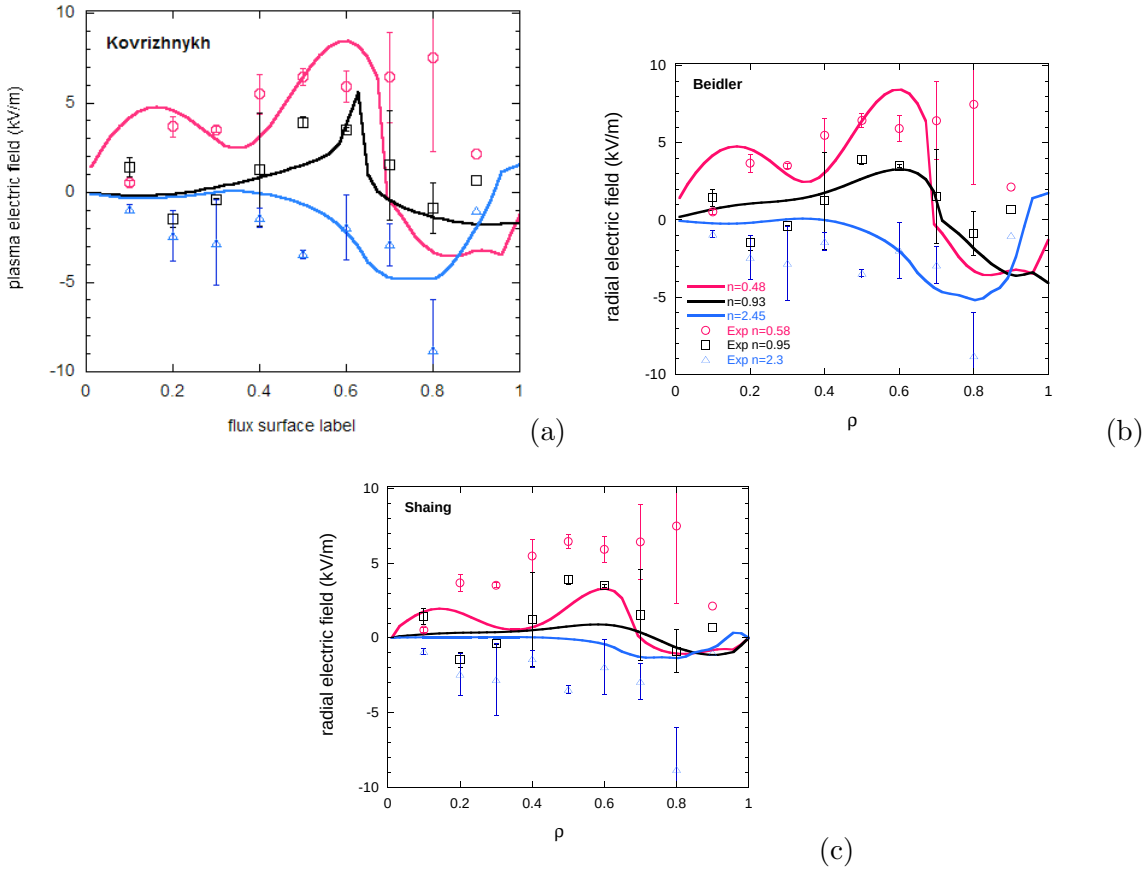

Figure 5. (a) E_r profiles for the models of: (a) Kovrizhnykh, (b) Beidler and (c) Shaing calculated for three experimental profiles from Fig. 2 for different line densities corresponding to the LDHT (cyan lines, $\overline{n} = 0.48 \times 10^19 m^{-3}$), IDT (black lines, $\overline{n} = 0.95$) and HDLT (blue lines, $\overline{n} = 2.45$) regimes; experimental profiles for line densities in the same regimes are shown with symbols and error bars.

4.2. Results of algebraic calculations.
The roots of Eq. (7) provide the radial electric field profile and the plasma potential profiles, $\phi(\rho)$, are obtained from $E_r(\rho)$ after radial integration from the edge to the magnetic surface at ρ, imposing the constraint $\phi(a) = 0$. The results for the E_r-profiles in each case are shown in Fig. 7(a), while the plasma potential profiles are shown in Fig. 7(b) (cf. Fig. 1), where they are compared with experimental results from each regime. It is seen that the same general features obtained with the semi-analytical models are also reproduced, approximately matching the experimental profiles, in particular, the sign change of E_r in the IDT regime at some radial position.

A common feature, already observed for TJ-II ECH plasmas [21], is that the plasma parameters for which the electric field is inverted in passing from LDHT to HDLT plasmas – the IDT regime discussed above – are found in the interval $0.5 < (n_0/10^{19}) < 2$ in agreement with the experiments, which corresponds to local collisionalities $\nu^* \sim 0.01$. It should be stressed then that the basic NC model, even for the complicated geometry of the TJ-II Heliac-type stellarator, provides a reasonable first approximation for the main experimental results shown. The correlation with experimental data shown in Fig. 7(b) indicates that the plasma potential has dependencies related mainly with the plasma parameters and the peculiarities of transport.

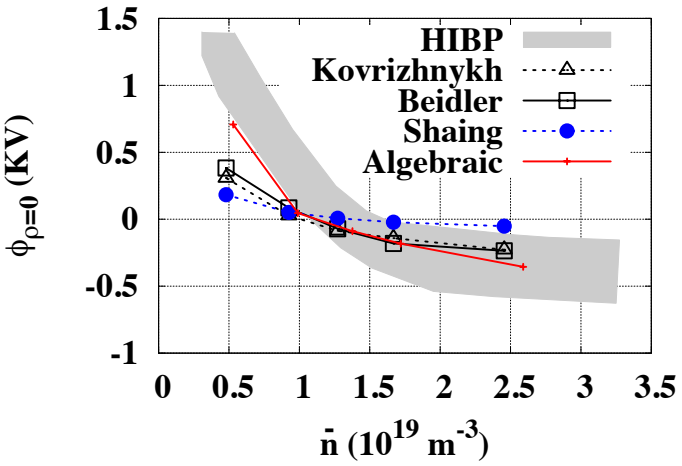

Figure 6. Plasma potential at the center obtained for Beidler, Kovrizhnikh, and Shaing models using the average experimental density and temperature profiles of Fig. 2. The analytical result is shown by the curve without symbols. Shaded area shows the range covered by the experimental values.

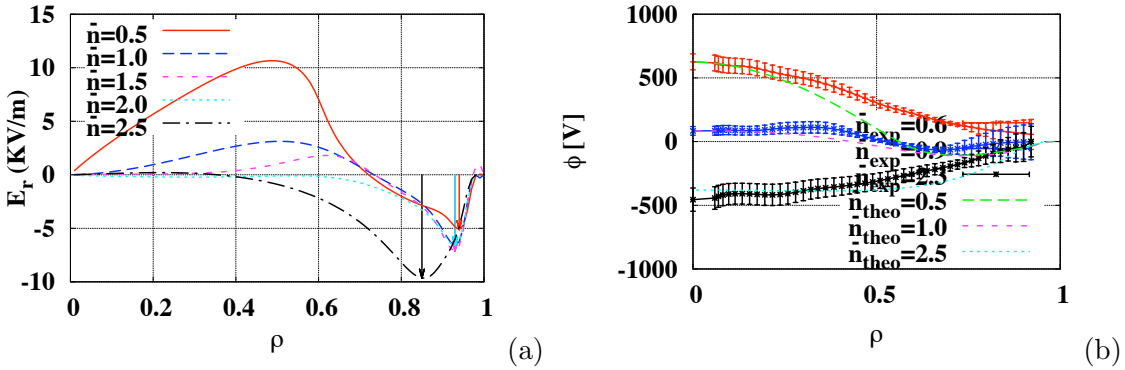

Figure 7. (a) E_r profiles from algebraic model using the five densities for model profiles in Figs. 3(b) and 4 going from LDHT to HDLT regimes; (b) ϕ profiles for the same model proflies, showing also the experimental profiles from HIBP for three densities for comparison, marked with symbols.

5. Discussion

In the light of the results obtained from our computations with the different approaches and models and compared with the HIBP measurements, we can make an appraisal of the role of NC transport regarding the radial electric fields. The main results of the comparison between experimental measurements and theoretical modeling are captured in figures 5 and 6. Figure 5 shows that both, experimental and theoretical E_r-profiles, approach to negative values as the density increases from the lowest values; in particular, a dip in E_r begins to develop near the edge ($\rho \sim 0.8$) when n rises, prior to becoming negative (also seen in Fig. 7). This is a systematic behavior in TJ-II plasmas that we find well described by the models. However, on the quantitative side, we find that the experimental data yield stronger fields than the models, in particular for the extreme LDHT and HDLT cases. This is apparent in figure 6, for the central potential: the crossing to negative values seems reasonably well represented by the models but the high (low) potentials at low (high) density are in general underestimated. On this respect

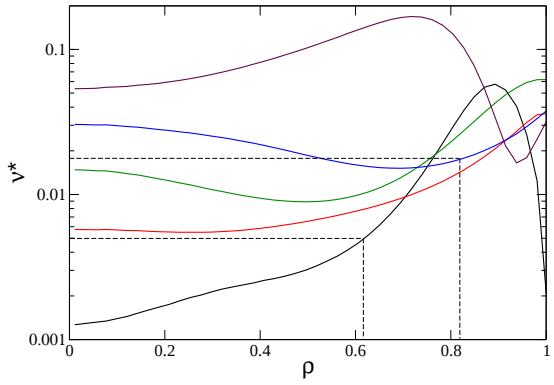

Figure 8. Collisionality profiles for the plasma profiles in Fig. 2 from discharge #15585, showing the collisionality range where E_r changes sign.

we must remember the simplifications of NC theory not accounted for in the models. In TJ-II, there are significant populations of supra-thermal electrons in LDHT conditions [23, 24, 25]. Furthermore, a low density transition to better particle confinement has been identified with the establishment of negative electric fields near the edge and the drastic drop of high energy (> 20 keV) radiation from brehmsstrahlung [26]. Therefore, the presence of fast electrons and ECH pump-out effects are likely candidates to explain why the plasma electric potential presents higher $\phi(0)$ than the models, where these effects are not accounted for. In the case of the high density plasmas, it seems also the case that NC calculations considering the magnetic geometry in more detail yield lower electric fields than measured. It has been argued that this is due to non-local effects related with large-width banana orbits for the ions in TJ-II plasmas [27, 28]. The fact might be more general according to a recent benchmarking effort between numerical NC calculations and experimental data [1]. In general, then, the semi-analytical models behave quite like their numerical counterparts based on Montecarlo or other techniques.

Comparing the E_r profiles from the three models for experimental profiles we notice a general agreement among them, with Beidler and Kovrizhnykh models giving quite similar results—and reasonably close to the experimental data—and Shaing model yielding smaller values of the electric field and plasma potential in the extreme density cases. This consistency among models together with the fair comparison with the experiment indicates the robustness of the main assumptions of NC transport, which is remarkable in the complicated geometry of the TJ-II stellarator.

Once the models have been found acceptable to represent the radial electric field, we turn to the interpretation of some general properties of TJ-II plasmas. The transition from the LDHT regime to the IDT regime in TJ-II plasmas is characterized by a change in plasma rotation that gives rise to an $E \times B$-flow shearing layer near the edge; in particular, the rotation velocity reverses where the electric field changes sign. We analyze this fact in terms of the plasma collisionality. In Fig. 8 the collisionality profiles are plotted for the cases of experimental profiles (Fig. (2)) from the LDHT to the HDLT regimes and as one can see they have different behavior; near the center they are increasing with ρ for low $\overline{n}$ and decreasing for high $\overline{n}$. However, the radial position where the electric field changes sign, which is marked with the lines, always falls within a limited collisionality range. This means that, for all profile types, when the collisionality exceeds a certain value, trapped electrons become less important than circulating ions and there is a transition from the electron to the ion root.

The agreement of the algebraic model with the rest of the models seen in Fig. 6 points again to the robustness of the neoclassical particle fluxes in predicting the electric fields. There is also

a qualitative agreement for the profiles as it is clear by comparing figures 7 and 5. Therefore, we can use the neoclassical formulation to study in more detail the passage from the LDHT regime to the IDT.

When a low density ECRH plasma in TJ-II evolves to a higher density via external gas puffing, the plasma rotation starts changing sign near the edge but inside the plasma [7]. To analyze this behavior, first we must note that, for a given E_r, the electron and ion fluxes change with collisionality at different rates. For low collisionalities Montecarlo calculations [29] show that $\partial_\nu \Gamma_i > \partial_\nu \Gamma_e$, *around the point where* $\Gamma_e = \Gamma_i$. This implies that, when ν is slightly increased (as when the density is increased by gas puffing) from its value for ambipolarity, $\Gamma_i > \Gamma_e$ which produces $\partial_t E_r < 0$, according to Eq. 3. The same relationship is satisfied for the fluxes with the algebraic model. Hence, for low collisionality (when $E_r > 0$), the electric field decreases when the density is raised. However, we may ask why there should be some $\rho < 1$ where the electric field drops faster and hits first the negative values. A typical observation is that the collisionality in low density plasmas shows a maximum around $\rho = 0.8 - 0.9$ and we hypothesize that this is related to the radius of the E_r inversion.

This hypothesis seems to be supported by simulations of TJ-II discharge #15585 (see figure 1(a)), shown in figure 9 giving the profile evolution of (a) the radial electric field and (b) the collisionality. For this simulation, ECE data have been used to build the evolving T_e-profile, while the density profiles have been constructed using a typical low density shape re-scaled to give the known line density. The collisionality shows a maximum near $\rho = 0.8$, which is the radial location where a dip in $E_r(\rho)$ develops and eventually becomes negative. Therefore, neoclassical transport suggests that the E_r inversion occurs at the maximum of collisionallity.

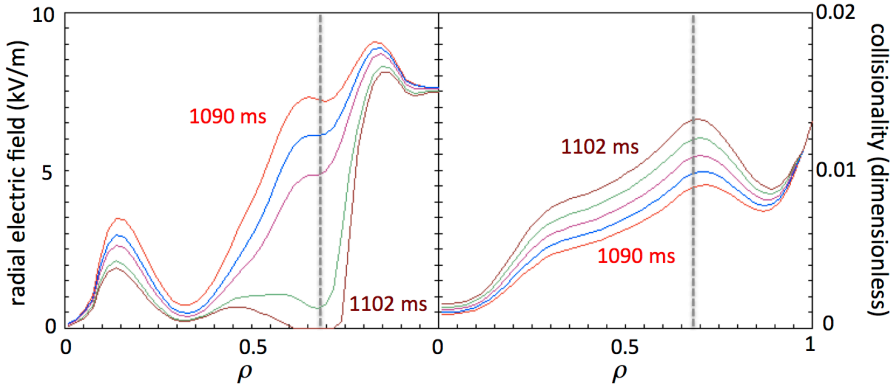

Figure 9. (a) Simulated evolution of a plasma from the LDHT to the IDL regimes where the line density evolves as is in TJ-II discharge #15585 (see Fig. 1(a)). The evolution of the radial electric field according to Kovrizhnykh semi-analytical model showing that it becomes zero at $\rho \approx 0.7$. (b) Corresponding collisionality has a maximum at the same position and increases with time since density increases and the electron temperature decreases.

It is interesting to analyze the equilibrium point for $E_r = 0$ from the point of view of rotation dynamics. In [30] it is shown that the transition from the electron to the ion root occurs in a poloidal rotation shear layer, where E_r can be obtained from a diffusion equation which may be interpreted as a balance between the non-ambipolar flux $e(Z_i\Gamma_i - \Gamma_e)$ and a viscous particle flux, driven by a poloidal viscous force,

$$\Gamma_{vis} \equiv \frac{2}{r^2}\frac{d}{dr}\left[r^2\hat{\eta}\left(E_r' - \frac{1}{r}E_r\right)\right] - \frac{\partial\hat{\eta}}{\partial E_r}\left(E_r' - \frac{1}{r}E_r\right)^2 = e(Z_i\Gamma_i - \Gamma_e), \tag{8}$$

where $\hat{\eta}$ is a viscosity coefficient. From here, we see that an ambipolar equilibrium ($e(Z_i\Gamma_i = \Gamma_e)$) can be reached at a point with $\rho < 1$ for vanishing E_r, when the $E_r(\rho)$ profile has a minimum (i.e. $E_r' = 0$) there, as in the left panel of Fig. 9. In that case $\Gamma_{vis} = 0$, which means that the viscous stress vanishes at the point where the poloidal rotation starts to change direction. This is in agreement with what was found in Ref.[31].

Finally, we turn to the problem of the formation of transport barriers in non-axisymmetric devices from the neoclassical viewpoint. In such devices the L-H transition happens at different rates, possibly due to the fact that the transport barriers can develop inside the plasma (instead of right at the plasma edge, as is normally the case in tokamaks) where neoclassical fluxes are not negligible in comparison with their anomalous counterpart. Assuming the paradigm of turbulence quenching due to the establishment of sheared electric drifts, it is in order asking whether the neoclassical electric field can provide a positive feedback loop for the establishment of a robust transport barrier. In other words: will the neoclassical E_r respond to the increasing gradients developing a stronger shearing rate in the $E \times B$ flows? This would give a positive feedback mechanism of the kind studied, e.g., in ref. [32], where the increasing pressure gradient intensifies the shearing rate that, in turn, eases a further increment of the pressure gradient. The models used in this paper provide such positive feedback indeed.

6. Conclusions

The results of calculations of the E_r field from the framework of neoclassical transport theory have been compared with experimental measurements of the plasma potential obtained with HIBP diagnostics in the TJ-II stellarator. Different collisionality regimes were analyzed with several theoretical models which in general terms yield E_r profiles in agreement with the experiment, indicating that neoclassical theory is a reasonable description for non-ambipolar fluxes [16]. However, the absolute values of the NC fluxes are smaller than the actual ones. From experimental observations, we can define three characteristic intervals for density and electron temperature. From the comparison of analytical results with results obtained from the three described models for the neoclassical fluxes, it can be noted that Kovrizhnykh and Beidler models are more adequate to model the non-axisymmetric NC transport in TJ-II plasmas (6), in the sense that solutions to the ambipolar equation (2) are closer to the experimental measurements and to those of the analytical model, which is entirely based on asymmetric NC transport. The qualitative agreement with experimental E_r profiles is remarkable considering that, for this model a simple magnetic geometry with a single helical harmonic (4), was assumed, with a simplified representation of helical ripple that is varied to improve the fits (Eq. 5). In the case of Beidler model, in a low collisionality regime we note it yields larger values than the other semi-analytical models (notice that the analytical fits of NC fluxes to the numerical DKES results, used in this model, deviate from them for small collision frequencies [18]).

Multiple solutions of the electric field that satisfy the ambipolar constraint (2) often arise when particle fluxes have a nonlinear dependence on electric field. This problem can be solved when the constants involved in density and temperature profiles are chosen to satisfy two criteria: the existence of a stable plasma equilibrium $\overline{P} = \overline{n_e T_e} \approx$ const over different density regimes, and the existence of a single real solution for the ambipolar equation (enforcing ambipolarity on each flux surface) [33]. The roots of E_r depend upon the plasma profiles for density and the two temperatures, thus allowing to conclude that the jumps between roots at two neighboring radii at steady-state, can be controlled by the plasma parameter profiles.

For the case LDHT we confirm the fact that with centrally peaked temperature profiles, a large positive "electron root" radial electric field is observed. In some cases, it can lead to the formation of an internal transport barrier which has been collectivelly named core electron root confinement (CERC); the large E_r has the effect of reducing the neoclassical transport by driving both plasma species out of the high-loss "$1/\nu*$" regime[33]. In the case of HDLT, we also

obtain that the electric field becomes more negative near the plasma edge as was reported in other stellarators, with NBI heating. In general, the magnitude of the calculated E_r is smaller than HIBP measurements. Possible reasons are the presence of suprathermal particles since they would enhance the electric field, and non-local effects not accounted for in the theoretical models [34].

An important result is that the transition from the electron to the ion root is found to occur for a certain narrow range of collisionality which points to a threshold collisionality as the cause for the transition. The implication of this is that a right amount of collisions, which destroy the trapped particle orbits that produce large electron losses, is responsible for the appearance of the ion root. The determination of the change in the radial electric field sign as a function of collisions (see Fig. 8) could have a strong influence in the transport barrier formation [35].

The good performance of the analytical NC model in predicting E_r was exploited to explain the observation that E_r gets zero inside the plasma edge in going to from LDHT to IDT regimes. It was shown that this occurs where the collision frequency profile has a maximum. The maximum in turn would produce an accelerated reduction of E_r in a given low collisionality range. The NC model also provides support to the idea that an improved confinement mode can be maintained by the increased sheared $E \times B$ flows.

Acknowledgments: Partial support from projects PAPIIT-UNAM IN106911 and Conacyt 152905 is acknowledged.

[1] Dinklage A., Yokoyama M., Tanaka K., et al., 2013 *Nucl. Fusion* **53** 063022.
[2] Chmyga A.A., Dreval N.B., Khrebtov S.M., et al., 2002 *29th EPS Conf. Plasma Physics*, Montreaux, ECA Vol. 26B, O-1.09.
[3] Hidalgo C., et al., 2005 *Nucl. Fusion*, **45**, S266-S275.
[4] Garcia J., Dies J., Castejon F., et al., 2007 *Phys. Plasmas* **14** 102511.
[5] Vargas V.I, Lopez-Bruna D., Garcia J., et al., 2008 *35th EPS Conf. Plasma Physics*, Hersonissos, ECA Vol. 32D, P-5.018.
[6] Bondarenko I.S., et al., 2000 *Czech. J. Phys.* **50** 1397.
[7] Happel T., Estrada T. and Hidalgo C., 2008 *Europhys. Lett.* **84** 65001.
[8] Hidalgo C., Pedrosa M.A., Castellano J., et al., 2001 *Plasma Phys. Controll. Fusion* **43** A313.
[9] Baciero A., Zurro B., McCarthy K.J., et al., 2001 *Rev. Sci. Instrum.* **72** 971–974.
[10] Herranz J., et al., 2000 *Phys. Rev. Lett.* **85** 4715.
[11] van Milligen B.Ph., 2011 *Rev. Sci. Instrum.* **82** 073503.
[12] Shaing K. C., 1984 *Phys. Fluids* **27** 1567.
[13] Hastings D.E., Houlberg W.A., Shaing K.C., 1985 *Nucl. Fusion* **25** 445 .
[14] Kovrizhnykh L.M., 1999 *Plasma Phys. Rep.* **25** 760.
[15] Hinton F.L., Hazeline R.D., 1976 *Rev. Mod. Phys.* **48** 239.
[16] Turkin Yu., Beidler C.D., Maasberg H., et al., 2011 *Phys. Plasmas* **18** 022505.
[17] Kovrizhnykh L.M., 2005 *Plasma Phys. Rep.* **31** 14.
[18] Maasberg H., Beidler C.D., Simmet E.E., 1999 *Plasma Phys. Contr. Fusion* **41** 1135.
[19] Beidler C.D., 1996 *Neoclassical transport properties of HSR*, IPP-Report 2/331, p.194.
[20] Kovrizhnykh L.M., 2006 *Plasma Phys. Rep.* **32** 988 .
[21] López-Bruna D., Reynolds J.M., Cappa A., et al. 2010 *Programas Periféricos de ASTRA para el TJ-II.* Informes Técnicos Ciemat 1201.
[22] Pereverzev G.V., Yushmanov P.N., 2002 ASTRA *Automated System for TRansport Analysis*, Max-Plank-Institute für Plasmaphysik Rep IPP 5/98 Garching.
[23] Medina F., et al., 2001 *Rev. Sci. Instrum.* **72** 471.
[24] Ochando M.A., et al., 2003 *Plasma Phys. Control. Fusion* **45** 221.
[25] Ochando M.A., et al., 2006 *Plasma Phys. Control. Fusion* **48** 1573.
[26] Vargas V.I., et al., 2009 *Density dependence of particle transport in ECH plasmas of the TJ-II stellarator*, Informes Técnicos Ciemat No. 1162.
[27] López-Bruna D., Velasco J.L., Ochando M., et al., 2013 *Plasma Phys. Contrl. Fusion*, **55**, 015001.
[28] Velasco J.L., Castejon F., Tarancon A., 2009 *Physics of Plasmas*, **16**, 052303.
[29] Tribaldos V., 2001 *Phys. Plasmas* **8** 1229.
[30] Maassberg H et al., 1993 *Phys. Fluids B* **5** 3627.
[31] Velasco J.L. et al., 2012 *Phys. Rev. Lett.* **109** 135003.

[32] Carreras, B.A., et al., 1994 *Plasma Phys. Control. Fusion* **36** A93.
[33] Lore J., Guttenfelder W., Briesemeister A., et al., 2010 *Phys. Plasmas* **17** 056101.
[34] Tribaldos, V., Guasp, J., 2005 *Plasma Phys. Control. Fusion,***47** 545 .
[35] Idei H., Ida K., Sanuki H., et al., 1993 *Phys. Rev. Lett.* **71** 2220.